

NOTICE: This is the author's version of a work accepted for publication by Elsevier. Changes resulting from the publishing process, including peer review, editing, corrections, structural formatting and other quality control mechanisms, may not be reflected in this document. Changes may have been made to this work since it was submitted for publication. A definitive version was subsequently published in *Electrochimica Acta*, Vol. 54, 2009, [doi:10.1016/j.electacta.2009.02.079](https://doi.org/10.1016/j.electacta.2009.02.079).

**Excess power and the product molecular hydrino  $H_2(1/4)$  generated in a  $K_2CO_3$   
electrolysis cell**

**R. L. Mills\*, W. Good, J. He**

BlackLight Power, Inc.

493 Old Trenton Road

Cranbury, NJ 08512

**ABSTRACT**

Novel inorganic hydride compounds  $KHKHCO_3$  and  $KH$  were isolated and characterized following the highly exothermic electrolysis of a  $K_2CO_3$  electrolyte, and the hydride was shown to comprise hydrino hydride ions [R. Mills, E. Dayalan, P. Ray, B. Dhandapani, J. He, *Electrochim. Acta* 47 (2002) 3909; R. Mills, *Int. J. Hydrogen Energy* 25 (2000) 669; R. Mills, J. New Mat. Electrochem. Sys. 6 (2003) 45; R. Mills, *Fusion Technology*, Vol. 37, No. 2, (2000), 157-182.]. We report further evidence of the catalysis of hydrogen to form molecular hydrino with potassium catalyst in a  $K_2CO_3$  electrolytic cell. Excess enthalpy of a factor of 40% that of the ohmic power dissipation was observed.  $H_2(1/4)$ , molecular hydrogen in a fractional Rydberg state, was predicted as a further product. From the NMR frequency, the energy state of the molecular hydrogen can be measured. The electrolysis gas was collected in a hollow nickel cathode that permitted enrichment of  $H_2(1/4)$  based on its higher mobility. The gases were dissolved in  $CDCl_3$  and characterized by  $^1H$  NMR. A singlet peak upfield of  $H_2$  was observed with the predicted chemical shift of 1.25 ppm relative to tetramethylsilane (TMS). The

---

\* Phone: 609-490-1090, Fax: 609-490-1066; e-mail: [rmills@blacklightpower.com](mailto:rmills@blacklightpower.com)

$H_2$  (1/4) NMR peak was further observed on samples prepared by dissolving each of the crystals that precipitated from the electrolyte and concentrated electrolyte in  $CDCl_3$ .

Keywords: electrolysis, exothermic catalysis reaction, molecular hydrino, NMR

## 1. Introduction

In addition to the observables on the hydrogen atom that are known, the laws of classical physics predicts [5-16] that atomic hydrogen may undergo a catalytic reaction with certain atomized elements and ions which singly or multiply ionize at integer multiples of the potential energy of atomic hydrogen,  $m \cdot 27.2 \text{ eV}$  wherein  $m$  is an integer. The predicted reaction involves a resonant, nonradiative energy transfer from otherwise stable atomic hydrogen to the catalyst capable of accepting the energy. The product is  $H(1/p)$ , fractional Rydberg states of atomic hydrogen called “hydrino atoms” wherein  $n = \frac{1}{2}, \frac{1}{3}, \frac{1}{4}, \dots, \frac{1}{p}$  ( $p \leq 137$  is an integer) replaces the well-known parameter  $n = \text{integer}$  in the Rydberg equation for hydrogen excited states.

Specifically, the Rydberg equation for the principal energy levels of atomic hydrogen is given by

$$E_n = -\frac{e^2}{n^2 8\pi\epsilon_0 a_H} = -\frac{13.598 \text{ eV}}{n^2} \quad (1a)$$

$$n = 1, 2, 3, \dots \quad (1b)$$

where  $e$  is the elementary charge,  $\epsilon_0$  is the permittivity of vacuum, and  $a_H$  is the radius of the hydrogen atom. The excited energy states of atomic hydrogen are given by Eq. (1a) for  $n > 1$  in Eq. (1b). The  $n = 1$  state is the “ground” state for “pure” photon transitions (i.e. the  $n = 1$  state can absorb a photon and go to an excited electronic state, but it cannot release a photon and go to a lower-energy electronic state). However, an electron transition from the ground state to a lower-energy state is possible by a resonant nonradiative energy transfer such as multipole coupling or a resonant collision mechanism. Processes such as hydrogen molecular bond formation that occur without photons and that require collisions are common [17]. Also, some commercial phosphors are based on resonant nonradiative energy transfer involving multipole coupling [18]. The reaction involves a nonradiative energy transfer followed by characteristic continuum emission [19] or energy transfer to H to form extraordinarily hot, excited-state H [19-27] and a hydrogen atom that is lower in energy than unreacted atomic hydrogen that corresponds to a fractional principal quantum number given by

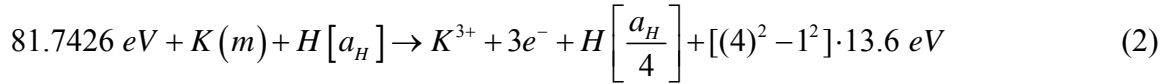
$$n = 1, \frac{1}{2}, \frac{1}{3}, \frac{1}{4}, \dots, \frac{1}{p}; \quad p \leq 137 \text{ is an integer} \quad (1c)$$

in Eq. (1a). The  $n = 1$  state of hydrogen and the  $n = \frac{1}{\text{integer}}$  states of hydrogen are nonradiative,

but a transition between two nonradiative states, say  $n = 1$  to  $n = 1/4$ , is possible via a nonradiative energy transfer. Thus, a catalyst provides a net positive enthalpy of reaction of  $m \times 27.2 \text{ eV}$  (i.e. it resonantly accepts the nonradiative energy transfer from hydrogen atoms and

releases the energy to the surroundings to affect electronic transitions to fractional quantum energy levels). As a consequence of the nonradiative energy transfer, the hydrogen atom becomes unstable and emits further energy until it achieves a lower-energy nonradiative state having a principal energy level given by Eqs. (1a) and (1c).

One such atomic catalytic system involves potassium since the reaction  $K$  to  $K^{3+}$  provides a net enthalpy equal to  $3 \cdot 27.2 \text{ eV}$ . The balanced reaction for  $K$  is



And, the overall reaction is



The energy given off during catalysis is much greater than the energy lost to the catalyst, and the energy released is large as compared to conventional chemical reactions. For example, when hydrogen and oxygen gases undergo combustion to form water



the known enthalpy of formation of water is  $\Delta H_f = -286 \text{ kJ/mole}$  or  $1.48 \text{ eV}$  per hydrogen atom. By contrast, each ( $n = 1$ ) ordinary hydrogen atom undergoing a catalysis step to  $n = \frac{1}{4}$  (Eqs. (2)–(4)) releases a net of  $204 \text{ eV}$ . The product  $H(1/4)$  (designated in abbreviated form) may further react to form the corresponding hydrino hydride ion  $H^-(1/4)$  or molecular hydrino  $H_2(1/4)$ . Consider the latter case. In general, the  $^1H$  NMR resonance of  $H_2(1/p)$  is predicted to be upfield from that of  $H_2$  due to the fractional radius in elliptic coordinates [5, 9] wherein the electrons are significantly closer to the nuclei. The predicted shift,  $\frac{\Delta B_T}{B}$ , for  $H_2(1/p)$  derived previously [5, 9] is given by the sum of that of  $H_2$  and a term that depends on  $p = \text{integer} > 1$  for  $H_2(1/p)$ :

$$\frac{\Delta B_T}{B} = -\mu_0 \left( 4 - \sqrt{2} \ln \frac{\sqrt{2} + 1}{\sqrt{2} - 1} \right) \frac{e^2}{36a_0m_e} (1 + \pi\alpha p) \quad (6)$$

$$\frac{\Delta B_T}{B} = -(28.01 + 0.64p) \text{ ppm} \quad (7)$$

where for  $H_2$   $p = 0$ . The experimental absolute  $H_2$  gas-phase resonance shift of  $-28.0 \text{ ppm}$  [28–31] is in excellent agreement with the predicted absolute gas-phase shift of  $-28.01 \text{ ppm}$  (Eq. (7)).

Some prior related studies demonstrating the hydrino reaction and products such as  $H^-(1/4)$  and  $H_2(1/4)$  from  $K$  and other catalysts include extreme ultraviolet (EUV) spectroscopy, characteristic emission from catalysts and the hydride ion products, lower-energy

hydrogen emission, chemically formed plasmas, Balmer  $\alpha$  line broadening, population inversion of H lines, elevated electron temperature, anomalous plasma afterglow duration, power generation, and analysis of novel chemical compounds [19-27, 32-53]. Since atomic hydrogen and  $K$  atoms are formed by reduction at the cathode of an aqueous  $K_2CO_3$  electrolysis cell and the  $K$  atoms contact the atomic hydrogen at the cathode, the catalysis of atomic hydrogen to form hydrinos was predicted to occur in these cells as well. It was previously reported that calorimetry of pulsed current and continuous electrolysis of aqueous potassium carbonate at a nickel cathode performed by Thermacore, Inc. [54] showed excess power out of 41 W that exceeded the total input power given by the product of the electrolysis voltage and current by a factor greater than 8. Novel inorganic hydride compounds  $KHKHCO_3$  and  $KH$  were isolated following the electrolysis of a  $K_2CO_3$  electrolyte. The compounds which comprised high binding energy hydride ions were stable in water, and  $KH$  was stable at elevated temperature (600 °C). Inorganic hydride clusters  $K[KHKHCO_3]_n^+$  were identified by positive Time of Flight Secondary Ion Mass Spectroscopy (ToF-SIMS) of  $KHKHCO_3$  [1-4]. The negative ToF-SIMS was dominated by hydride ions. The positive and negative ToF-SIMS of  $KH$  showed essentially  $K^+$  and  $H^-$  only, respectively. Moreover, the existence of novel hydride ions was determined using X-ray photoelectron spectroscopy, and  $^1H$  nuclear magnetic resonance spectroscopy.

We report further evidence of the catalysis of hydrogen to lower energy states with potassium in a  $K_2CO_3$  electrolytic cell. In this paper, we report the observation of excess power corresponding to the exothermic reaction to form H states given by Eqs. (1a) and (1c) by measuring the temperature of the electrolyte for a given input electrolysis power compared to the heat loss of the electrolyte using a resistive heater.  $H_2(1/4)$  formed from the product  $H(1/4)$  has an internuclear distance of 1/4 that of  $H_2$ ; thus, it is predicted to have a higher mobility through metals than  $H_2$ . This provided a means to enrich and isolate  $H_2(1/4)$  by differential diffusion through a hollow nickel cathode. The collected gas was dissolved in  $CDCl_3$  and characterized by  $^1H$  NMR which has the capability to measure the energy state of hydrogen according to Eqs. (6)–(7) wherein the predicted chemical shift of  $H_2(1/4)$  corresponds to  $p = 4$ . The crystals that precipitated from the electrolyte and concentrated electrolyte were also dissolved in  $CDCl_3$ , and the NMR was recorded to further identify  $H_2(1/4)$  in these samples.

## 2. Experimental

### 2.1. Calorimetry on electrolysis cells

#### 2.1.1. Power balance

The power balance of the electrolytic cells was measured calorimetrically using a Calvet calorimeter (International Thermal Instruments) shown in Fig. 1. The cylindrical calorimeter walls contained a thermopile structure composed of two sets of thermoelectric junctions. One set of junctions was in thermal contact with the internal calorimeter wall, at temperature  $T_i$ , and the second set of thermal junctions was in thermal contact with the external calorimeter wall at  $T_{ext}$  which was held at a constant temperature. When heat was generated in the calorimeter cell, the calorimeter radially transferred a constant fraction of this heat into the surrounding heat sink. As heat flowed a temperature gradient,  $(T_i - T_{ext})$ , was established between the two sets of thermopile junctions. This temperature gradient generated a voltage that was compared to the linear voltage versus power calibration curve to give the power. The calorimeter was calibrated “on-the-fly” by the addition of known quantities of joule heat (thermal power) during the electrolysis. Power was added with an array of four resistors that served as a joule heater and a fixed power source. The calibration constant of the Calvet calorimeter was not sensitive to the range of powers studied. To maintain an isothermal reaction system and improve baseline stability, the calorimeter was placed inside a commercial forced-convection refrigerator that maintained the temperature constant at  $15^\circ\text{C} \pm 0.1^\circ\text{C}$  over 24 hours. A more complete description of the methods is given in Bradford et al. [55].

The general form of the energy balance equation for the cell in steady state is:

$$0 = P_{appl} + Q_{htr} + Q_{xs} - P_{gas} - Q_{loss} \quad (8)$$

where  $P_{appl}$  is the electrolysis power applied to the cell;  $Q_{htr}$  is the power input to the heater;  $Q_{xs}$  is the excess heat power generated by the hydrogen catalysis reaction;  $P_{gas}$  is the power removed as a result of evolution of  $H_2$  and  $O_2$  gases, and  $Q_{loss}$  is the thermal power loss from the cell through the Calvet thermopiles. When an aqueous solution is electrolyzed to liberate hydrogen and oxygen gasses, the electrolysis power  $P_{appl}(= E_{appl}I)$  can be partitioned into two terms:

$$P_{appl} = E_{appl}I = P_{cell} + P_{gas} \quad (9)$$

An expression for  $P_{gas}(= E_{gas}I)$  is readily obtained from the known enthalpy of formation of water from its elements:

$$E_{gas} = \frac{-\Delta H_{form}}{\alpha F} \quad (10)$$

( $F$  is Faraday's constant), which yields  $E_{gas} = 1.48\text{V}$  for the reaction



The net Faradaic efficiency  $\eta$  of gas evolution is not assumed to be unity, but was measured.

Thus, Eq. (9) becomes

$$P_{cell} = E_{appl}I - 1.48 V\eta I \quad (12)$$

The cell was calibrated by supplying additional increments of thermal power to the cell using a resistance heater  $Q_{hr}$  while maintaining constant electrolysis and by inferring the Calvet calibration constant  $a$  from the linear fit of the output Calvet voltage  $V_c$  as a function of  $Q_{hr}$  where the heat losses were primarily conductive losses through the Calvet thermopiles. When the heater was off, the Calvet output is given by

$$V_c = a(P_{appl} + 0 + Q_{xs} - P_{gas}) + C \quad (13)$$

wherein  $C$  is a constant characteristic of the Calvet response. When a new steady state is established with the heater on, the power balance changes to:

$$V'_c = a(P'_{appl} + Q_{hr} + Q'_{xs} - P'_{gas}) + C' \quad (14)$$

where a prime superscript indicates a changed value when the heater was on. When the following assumptions apply

$$Q_{xs} = Q'_{xs}; P_{appl} = P'_{appl}; P_{gas} = P'_{gas}; C = C' \quad (15)$$

The Calvet calibration constant  $a$ , is given by the result

$$a = \frac{V'_c - V_c}{Q_{hr}} \quad (16)$$

In all heater power calculations, the following equation was used

$$Q_{hr} = E_{hr}I_{hr} \quad (17)$$

In the case of intermittent square-wave electrolysis,  $P_{appl}(t)$  of Eq. (9) was determined from the product of the voltage  $E_{appl}(t)$  and the current  $I(t)$  measured from the respective waveforms recorded with a 300 MHz oscilloscope. Since these measurements varied over the cycle, the product was integrated and divided by the period  $\Delta t$  to give

$$P_{appl}(t) = \frac{1}{\Delta t} \int E_{appl}(t)I(t)dt = \frac{1}{\Delta t} \int (P_{cell}(t) + P_{gas}(t))dt \quad (18)$$

In the case of intermittent square wave electrolysis with current only during the high voltage interval of the cycle ( $E_{appl} > 1.48V$ ) and where the net Faradaic efficiency of gas evolution  $\eta$  was measured,  $P_{cell}(t)$  of Eq. (12) becomes

$$P_{cell}(t) = \frac{1}{\Delta t} \int (E_{appl}(t)I(t) - 1.48V\eta I(t))dt \quad (19)$$

Using Eqs. (13)–(16), the Calvet calibration constant  $a$  and offset  $C$  were determined by applying increments of applied heating power where 24 hours was allowed for a steady state to be achieved in each case. First,  $a$  and  $C$  were determined without electrolysis input using the identical electrolysis cell wherein the applied power was to the heater only.  $a$  was given by the

slope of the plot of  $V_c$  versus heating power  $Q_{hr}$ , and  $C$  was given as the Calvet-voltage-axis intercept. Then,  $a$  and  $C$  were determined by addition of increments of heater power to the electrolytic cell wherein  $a$  was given by the slope of the plot of  $V_c$  versus total ohmic power given by the sum of  $Q_{hr}$  and  $P_{cell}$  with  $P_{appl}$ ,  $P_{gas}$ , and  $P_{cell}$  maintained constant and  $Q_{xs}$  assumed constant. Then, the total ohmic power  $P_T$  given by the sum

$$P_T = P_{appl} + Q_{hr} + Q_{xs} - P_{gas} = P_{cell} + Q_{hr} + Q_{xs} \quad (20)$$

was determined from the Calvet voltage:

$$P_T = \frac{V_c}{a} - C \quad (21)$$

And, the excess power was given by

$$Q_{xs} = P_T - P_{cell} - Q_{hr} \quad (22)$$

### 2.1.2. Electrolysis methods

The electrolysis cell comprised a 1.2 liter Pyrex vessel with a three-port cap filled with 700 ml of 0.6 molar potassium carbonate (Alfa  $K_2CO_3 \cdot 3/2H_2O$  99±%) electrolytic solution. The electrodes were completely submerged in the electrolyte. The cathode (Fig. 2) comprised 100 m of 0.38 mm diameter coiled nickel wire (99.8 % Alfa, cold drawn, clean Ni wire) wound around a support-frame of four Pyrex rods mounted into three rings of TFE having a total surface area of 1200 cm<sup>2</sup>. The anode (Fig. 2) comprised 7.5 m of 0.38 mm diameter coiled nickel wire (99.8 % Alfa, cold drawn, clean Ni wire) having 90 cm<sup>2</sup>. The cathode–anode separation distance was 1 cm. The nickel electrodes were cleaned by placing them in a beaker of 0.57 M  $K_2CO_3$ /10%  $H_2O_2$  for 30 minutes and then rinsing well with deionized water. The leads were inserted into Teflon tubes to minimize recombination of the evolving gases. The Pyrex vessel was sealed using a combination of silicon sealants (RTV 110 at top of two ports), an O-ring, and a Cajon fitting. The Cajon fitting allowed for the collection of electrolysis gas. A bubble flow meter was used to measure the gas production during the experiments.

As usual in electrochemistry, measures were taken to avoid impurities in the system, especially organic substances. The following procedures were applied in order to reproduce the excess heat effect. First, the electrolysis cell components were cleaned with Alconox then 0.1 M nitric acid and finally rinsed thoroughly with distilled water. The wire for the nickel wire cathode and anode was removed from its container with rubber gloves, and coiled in such a way that no organic substances were transferred to the nickel surface. The nickel cathode was dipped into the working solution under electrolysis current and never left in the working solution without electrolysis current.

The resistance heater used during calibration and operation comprised four 10 Ω 1% precision metal oxide resistors in a 2 mm outer diameter Teflon tube. The four resistors were

placed in an electrical circuit of total resistance  $10\ \Omega$  by placing two groups of two resistors in parallel. The calibration heater was powered by a constant power supply (Pennsylvania State University  $0\text{--}20\ \text{W} \pm 1\%$ ). The heating power was calculated using Eq. (17) as confirmation of the constant power.

The electrolysis power was applied either as constant current or pulsed current. The electrolysis voltage ( $\pm 0.05\%$ ) and current ( $\pm 0.05\%$ ), Calvet voltage ( $\pm 0.05\%$ ) and temperature  $T_{ext}$  ( $\pm 0.1\ ^\circ\text{C}$ ) data were acquired by a Labview data acquisition system. Data points were collected every 10 s and averaged over 5-min intervals. The precision of the measurements was 10V/16 bits. The measured voltages were compared to a Fluke 45 multimeter to ensure proper instrumental measurement. No discrepancies between the two were observed.  $P_{appl}$  was given by Eq. (9) as the product of the voltage and the constant current, and  $P_{cell}$  was given by Eq. (12).

The current of intermittent-electrolysis-power (pulsed-power) experiments was a periodic square-wave. The duty cycle, frequency, peak current (and thus voltage of electrolysis) were varied until a suitable set of conditions was found corresponding to the reported data. The electric power dissipated in the electrolysis cells was recorded with a 300 MHz digital oscilloscope (Tektronix TDS3034b). The voltage waveform was measured as the voltage drop across the leads to the electrodes at their point of entry into the Pyrex vessel. The current waveform was determined from an oscilloscope voltage measurement across a calibrated resistor ( $0.25\ \Omega$ ,  $1\%$ ) in series with the lead to the cathode. For all pulsed-power calculations,  $P_{appl}$  was determined from the product of the current waveform times the voltage waveform using Eq. (18), and  $P_{cell}$  was determined using Eq. (19). Once thermal equilibrium was achieved, the total input power to the electrolysis cell fluctuated less than 10 mW for the duration of the experiment.

The gas evolved during electrolysis was measured in a soap film flow meter using a stopwatch. Gas evolution rates ( $\pm 2\%$ ) were corrected for Barometric pressure, water vapor content, and temperature. Gas evolution data was analyzed for Faradaic efficiency,  $\eta$ .

## **2.2. $^1\text{H}$ NMR spectroscopy of gases that permeated the Ni tubing cathode during electrolysis of aqueous potassium carbonate**

Electrolysis was performed with aqueous potassium carbonate in a 350 ml vacuum jacketed dewar (Pope Scientific, Inc., Menomonee Falls, WI) with a platinum basket anode and a 170 cm long nickel tubing cathode (Ni 200 tubing, 0.159 cm O.D., 0.107 cm I.D., with a nominal wall thickness of 0.0254 cm, MicroGroup, Inc., Medway, MA). The cathode was coiled into a 3.0 cm long helix with a 2.0 cm diameter. One end of the cathode was weld-sealed above the electrolyte. The other end was connected to a gas collection system.

Sealed  $^1\text{H}$  NMR samples were prepared by collecting the electrolysis gases from the

hollow cathode in an NMR tube (5 mm OD, 23 cm length, Wilmad) that was then sealed. A port of an ultrahigh-vacuum borosilicate two-port valve was glass-blown joined to the NMR tube, and the valve-NMR-tube assembly was dried at 150°C for 12 h. 1 ml of  $CDCl_3$  (99.99% Cambridge isotopes) was transferred to the NMR tube with a syringe through the opened valve. An ultrahigh-vacuum-line connector attached a flexible stainless steel tube to the hollow cathode. The other end of the flexible tube was joined to the other port of the valve by an Ultratorr fitting. Electrolysis gases were collected in the hollow cathode that was initially evacuated to  $10^{-5}$  Torr. The two-port valve between the NMR tube and the hollow cathode was closed. The flexible tube was evacuated by opening a valve between vacuum-line connector and a turbo pump. The NMR tube was submerged in liquid nitrogen cryogen to two thirds of its length to fully immerse the NMR solvent. Then, the two-port valve was opened, and air was evacuated from the NMR tube by the vacuum pump. To remove trace, dissolved air, the two-port valve was closed. The cryogen was removed to allow the NMR solvent to warm up to room temperature. The NMR tube was submerged in cryogen, and it was evacuated again. Next, the valve to the vacuum pump was closed and the valve to the gas system was opened to allow the electrolysis gas to be condensed in the NMR tube containing NMR solvent. The NMR tube was on-line sealed with a propane torch.

Control NMR samples comprised ultrahigh purity hydrogen (Praxair) with NMR solvent. The sealed  $^1H$  NMR samples were prepared by connecting the NMR tube containing 1 ml of the NMR solvent to a vacuum line connected to the gas tanks. The NMR tube was submerged in cryogen to two thirds of its length to fully immerse the NMR solvent. With a tank isolation valve closed, the NMR tube was evacuated by a vacuum pump. After the valve to the vacuum pump was closed, the cryogen dewar was removed to allow the NMR solvent to come to room temperature. The NMR tube was then pressurized to 760 Torr with hydrogen that dissolved in the NMR solvent over 4-6 hours. The NMR tube was sealed with a propane torch.

Crystalline samples for solution NMR were also prepared. The crystals were isolated from the electrolytic cell by concentrating the  $K_2CO_3$  electrolyte about six fold using a rotary evaporator at 50 °C until a crystalline precipitate just formed. Additional electrolyte was added until the crystals just disappeared. Then, precipitated crystals of the suspension were grown over three weeks by allowing the saturated solution to stand in a sealed round bottom flask at 25°C. The crystals were added to NMR solvent to form a saturated solution, and the solution was decanted, sealed, and analyzed by NMR. 0.05 ml of the concentrated electrolyte was also added to the NMR solvent, and NMR was performed. The NMR spectra were recorded with a 300 MHz Bruker NMR spectrometer that was deuterium locked. The chemical shifts were referenced to the frequency of tetramethylsilane (TMS) at 0.00 ppm.

### 3. Results and discussion

#### 3.1. Power balance of the electrolysis cells

The Calvet voltage response to heater input power only ( $Q_{xs} = 0$ ,  $P_{appl} = 0$ ,  $P_{gas} = 0$ ) over the constant heater input power range of 0 W to 5 W was measured, and the results were used for a least-squares-fit determination of  $a$  and  $C$  of Eq. (13) as shown in Fig. 3. A summary of the  $K_2CO_3$  electrolysis parameters and power balance results with constant and intermittent current are summarized in Table 1. A higher Calvet voltage was produced at a given ohmic input when potassium carbonate electrolysis was performed compared to that of the heater alone that was representative of the excess power generated. The excess power  $Q_{xs}$  was calculated from Eqs. (21)–(22) using the measured  $V_c$ . The Faradaic efficiency of the constant-current electrolysis of  $K_2CO_3$  under the conditions of 1.72 amps and an applied voltage of 3.02 volts was 66% corresponding to  $\eta = 0.66$  in Eq. (12) and a  $P_{cell}$  of 3.51 W (Eq. (12)) and  $Q_{xs}$  of 0.550 W (Eqs. (21)–(22)). The excess power corresponded to a power gain of 16% of the ohmic input power.

The voltage and current waveforms for intermittent square-wave electrolysis recorded with a 300 MHz digital oscilloscope are shown in Fig. 4. The Calvet voltage versus total electrolysis ohmic input power ( $P_{cell} + Q_{htr}$ ) for potassium carbonate experiments also appears in Fig. 3. For pulsed-power experiments, at 10 Hz, 30% duty cycle, and 0.658 A peak current, no gas evolution was measured corresponding to  $\eta = 0$  in Eq. (19), and a  $P_{cell}$  of 0.460 W (Eq. (19)) and  $Q_{xs}$  of 0.184 W (Eqs. (21)–(22)).

The composition of the Ni cathode used in the aqueous potassium carbonate electrolyte was the same before and after the electrolysis (as determined by elemental analysis), and chemical analysis for potassium ion, carbonate ion, pH and specific gravity indicated no detectable change in the electrolyte as a result of the electrolysis. Thus, we conclude that excess heat and energy were produced in the electrolysis of aqueous potassium carbonate and that no chemical reaction involving the electrodes or the electrolyte is the source of that excess heat. Similar excess heat results have been reported by Mills [54, 56, 57] and others [54, 58]. These transitions are, apparently, taking place on the Ni cathode during the electrolysis of aqueous potassium carbonate. Atomic hydrogen is produced at the cathode surface during the electrolysis (part of the process of reducing  $H_2O$  to  $H_2$ ).  $K$  is also formed by reduction of  $K^+$ . The juxtaposition of the hydrogen atoms and potassium atoms on the cathode surface is an ideal configuration for the catalytic transition of hydrogen to hydrinos. The observed “excess heat” is, we suggest, a consequence of these atomic hydrogen transitions.

Neglect for the moment that  $H(1/4)$  can form a diatomic molecule  $H_2(1/4)$ . Eq. (4) predicts that 204 eV is released per H atom transition to the  $n = 1/4$  quantum state which

corresponds to 40 MJ/mol of  $H_2$ . In contrast, only 286 kJ is consumed by electrolyzing 1 mol of  $H_2O$  to produce 1 mol of  $H_2$  (Eq. (5)). Thus, the excess power of 550 mW produced by the  $K_2CO_3$  electrolytic cell as shown in Fig. 3 (which also produces 8.9  $\mu$ mol of  $H_2$  per second) could be accounted for by the conversion of at most 0.016% of the hydrogen atoms from the  $n = 1$  state to the  $n = 1/4$  state.

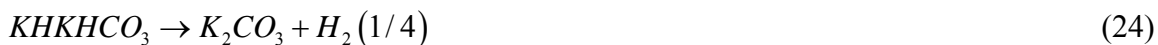
### 3.2. $^1H$ NMR

The  $^1H$  NMR spectrum on a sealed sample of  $K_2CO_3$  electrolysis gases dissolved in  $CDCl_3$  is shown in Fig. 5. The single peak of each of  $CDCl_3$  solvent,  $H_2$ , acetone, and  $H_2O$  was observed at their known chemical shifts: 7.26 ppm, 4.63 ppm, 2.18 ppm, and 1.54 ppm, respectively. The only peak in the spectra that could not be assigned to common species was the broad singlet peak upfield of  $H_2$  at 1.25 ppm that matched the theoretical position of  $H_2(1/4)$ . As expected for the hydrino reaction as the source of the  $H_2(1/4)$  peak, the 1.25 ppm peak was observed to increase with time of electrolysis. The solution-phase NMR of the electrolysis gas provides a definitive test of the theoretically predicted chemical shift of  $H_2(1/4)$ . Using Eq. (7) and the experimental absolute resonance shift of TMS,  $-31.5$  ppm [28-29], the predicted gas-phase shift of  $H_2(1/4)$  is

$$\frac{\Delta B_T}{B} = -30.6 \text{ ppm} - (-31.5 \text{ ppm}) = 0.9 \text{ ppm} \quad (23)$$

which is very close to the observed shift of 1.25 ppm shown in Fig. 5. No known common contaminant has a single singlet peaks at this position, the peak is distinguishable based on its large width, and this peak-position is also in good agreement with the  $^1H$  MAS NMR value of 1.13 ppm observed for  $H_2(1/4)$  in solid  $NaH * F$  and corresponding solution value of 1.25 ppm [19–20]. The large peak width in solution is indicative of strong interactions of  $H_2(1/4)$  with the matrix. Applicable relaxation interactions of  $H_2(1/4)$  with the solution that effect the line width such as nuclear magnetic dipole interactions due to high mobility and spin rotational interaction are given in Becker [59].

The electrolysis was run for long duration (18 months) in a large (28 l) cell [1–4]. The  $H_2(1/4)$  peak was further observed by dissolving each of the crystals that precipitated from the electrolyte (Fig. 6) and the concentrated electrolyte in NMR solvent (Fig. 7). The 1.25 ppm peak was observed to increase with concentration of crystallized electrolyte as well as the electrolyte. In addition to production of  $H_2(1/4)$  gas, these results on electrolytic samples demonstrate that  $H_2(1/4)$  was released from the inorganic hydrino-containing electrolysis products such as  $KHKHCO_3$  [1–4] by the decomposition reaction:



and is soluble in aqueous solution as well. Based on the previously observed large  $H_2(1/4)$  peak in DMF with the absence of a  $H_2$  peak [19, 20],  $H_2(1/4)$  solubility favors a polar solvent, and  $H_2$  shows the opposite trend. These are distinguishing physiochemical features of  $H_2(1/4)$  compared to  $H_2$ . The difference is also evident in the relative solution NMR peak widths.

#### 4. Conclusion

In this study we made specific theoretical predictions regarding the exothermic reaction to form  $H_2(1/4)$  and its characterization and tested them with standard, easily interpretable experiments. The results show that, as predicted, the new states of atomic and molecular hydrogen  $H(1/4)$  and  $H_2(1/4)$  are formed by reaction of hydrogen atoms with potassium atoms that serve as a hydrino-forming catalyst in a  $K_2CO_3$  electrolytic cell. Excess power was measured from the  $K_2CO_3$  electrolytic cell. Using a nickel wire cathode at a constant current of 1.72 A, production of excess power of 550 mW was observed that was 1.16 times  $P_{cell}$ . The power gain increased by applying the power intermittently as a periodic square-wave such that the total thermal output power of 644 mW exceeded  $P_{cell} = P_{appl}$  of 460 mW. The result could not be attributed to recombination of electrolysis gases or a previously known chemical reaction.

The electrolysis gas was isolated from a hollow cathode, dissolved in  $CDCl_3$ , and characterized by  $^1H$  NMR. A singlet peak upfield of  $H_2$  was observed with the predicted chemical shift of 1.25 ppm relative to tetramethylsilane (TMS). The  $H_2(1/4)$  peak was further observed by dissolving each of the crystals that precipitated from the electrolyte and the concentrated electrolyte in the NMR solvent demonstrating that  $H_2(1/4)$  was released from the inorganic hydrino-containing electrolysis products such as  $KHKHCO_3$  isolated and characterized previously [1–4] and is soluble in aqueous solution as well. The latter result with the absence of  $H_2$  from the crystals or the electrolyte and the prior observed higher solubility of  $H_2(1/4)$  in polar DMF compared to  $H_2$  demonstrates the unique physical properties of  $H_2(1/4)$  corresponding to its electronic state [19, 20]. The very large peak width of  $H_2(1/4)$  compared to  $H_2$  is another feature indicative of its physiochemical uniqueness from  $H_2$ .

These results confirmed the results of earlier studies reporting the characterizations of  $H^-(1/4)$  and  $H_2(1/4)$  as well as power and other signatures of the very exothermic reactions of their formation [19–27, 32–53]. Observational agreement with predicted positions of upfield-shifted  $^1H$  MAS NMR peaks, catalyst reactions, very high (>100 eV) H energies, substantial excess thermal energy, and spectroscopic data supports the present conclusion of the formation of  $H_2(1/4)$  by the  $K$  catalysis of  $H$ . The observation of excess enthalpy and the same 1/4

state of hydrogen, demonstrate that the hydrogen catalysis reaction occurs in liquid-solid interfacial environments as well as in the gas and solid phases [19–27, 32–53].

## References

1. R. Mills, E. Dayalan, P. Ray, B. Dhandapani, J. He, *Electrochim. Acta* 47 (2002) 3909.
2. R. Mills, *Int. J. Hydrogen Energy* 25 (2000) 669.
3. R. Mills, *J. New Mat. Electrochem. Sys.* 6 (2003) 45.
4. R. Mills, *Fusion Technology*, vol. 37, no. 2, March, (2000), pp. 157.
5. R. Mills, *The Grand Unified Theory of Classical Quantum Mechanics*; June 2008 Edition, posted at <http://www.blacklightpower.com/theory/bookdownload.shtml>.
6. R. L. Mills, *Phys. Essays* 16 (2003) 433.
7. R. Mills, *Phys. Essays* 20 (2007) 403.
8. R. L. Mills, *Phys. Essays* 18 (2005) 321.
9. R. L. Mills, *Phys. Essays* 17 (2004) 342.
10. R. L. Mills, *Phys. Essays* 19 (2006) 225.
11. R. L. Mills, *Phys. Essays* 21 (2008) 103.
12. R. L. Mills, *Annales de la Fondation Louis de Broglie* 30 (2005) 129.
13. R. Mills, *Int. J. Hydrogen Energy* 27 (2002) 565.
14. R. Mills, *Int. J. Hydrogen Energy* 26 (2001) 1059.
15. R. Mills, *Int. J. of Hydrogen Energy* 25 (2000) 1171.
16. R. Mills, “The Grand Unified Theory of Classical Quantum Mechanics,” Global Foundation, Inc. Orbis Scientiae entitled *The Role of Attractive and Repulsive Gravitational Forces in Cosmic Acceleration of Particles The Origin of the Cosmic Gamma Ray Bursts*, (29th Conference on High Energy Physics and Cosmology Since 1964) Dr. Behram N. Kursunoglu, Chairman, December 14–17, 2000, Lago Mar Resort, Fort Lauderdale, FL, Kluwer Academic/Plenum Publishers, New York, pp. 243.
17. N. V. Sidgwick, *The Chemical Elements and Their Compounds*, Volume I, Oxford, Clarendon Press, (1950), p.17.
18. M. D. Lamb, *Luminescence Spectroscopy*, Academic Press, London, (1978), p. 68.
19. R. L. Mills, Y. Lu, K. Akhtar, “Spectroscopic Observation of Helium-Ion- and Hydrogen-Catalyzed Hydrino Transitions,” submitted for publication.
20. R. L. Mills, G. Zhao, K. Akhtar, R. Chang, J. He, Y. Lu, W. Good, B. Dhandapani, *Int. J. Hydrogen Energy*, 34 (2009) 573.
21. R. L. Mills, P. Ray, B. Dhandapani, R. M. Mayo, J. He, *J. Appl. Phys.* 92 (2002) 7008.
22. R. L. Mills, P. Ray, B. Dhandapani, J. He, *IEEE Trans. Plasma Sci.* 31 (2003) 338.
23. R. L. Mills, P. Ray, *New J. Phys.* 4 (2002) 22.1.

24. R. L. Mills, B. Dhandapani, K. Akhtar, *Int. J. Hydrogen Energy* 33 (2008) 802.
25. R. Mills, P. Ray, B. Dhandapani, *J. Plasma Phys.* 72 (2006) 469.
26. J. Phillips, C-K Chen, K. Akhtar, B. Dhandapani, R. Mills, *Int. J. Hydrogen Energy* 32 (2007) 3010.
27. R. Mills, K. Akhtar, B. Dhandapani, "Tests of Features of Field-Acceleration Models for the Extraordinary Selective H Balmer  $\alpha$  Broadening in Certain Hydrogen Mixed Plasmas," submitted for publication.
28. K. K. Baldrige, J. S. Siegel, *J. Phys. Chem. A* 103 (1999) 4038.
29. J. Mason, Editor, *Multinuclear NMR*, Plenum Press, New York, (1987), (chapter 3).
30. C. Suarez, E. J. Nicholas, M. R. Bowman, *J. Phys. Chem. A* 107 (2003) 3024.
31. C. Suarez, *Chem. Educ.* 3, (1998) 1.
32. R. L. Mills, J. He, Y. Lu, M. Nansteel, Z. Chang, B. Dhandapani, *Int. J. Hydrogen Energy* 32 (2007) 2988.
33. R. Mills, J. He, Z. Chang, W. Good, Y. Lu, B. Dhandapani, *Int. J. Hydrogen Energy* 32 (2007) 2573.
34. R. Mills, P. Ray, B. Dhandapani, W. Good, P. Jansson, M. Nansteel, J. He, A. Voigt, *Eur. Phys. J. Appl. Phys.* 28 (2004) 83.
35. R. Mills and M. Nansteel, P. Ray, *IEEE Trans. Plasma Sci.* 30 (2002) 639.
36. R. Mills and M. Nansteel, P. Ray, *New J. Phys.* 4 (2002) 70.1.
37. R. Mills, J. Dong, Y. Lu, *Int. J. Hydrogen Energy* 25 (2000) 919-943.
38. R. Mills, M. Nansteel, P. Ray, *J. Plasma Phys.* 69 (2003) 131.
39. R. L. Mills, J. He, M. Nansteel, B. Dhandapani, *Int. J. Global Energy Issues (IJGEI)* 28 (2007) 304.
40. H. Conrads, R. Mills, Th. Wrubel, *Plasma Sources Sci. Technol.* 12 (2003) 389.
41. J. Phillips, R. L. Mills, X. Chen, *J. Appl. Phys.* 96 (2004) 3095.
42. R. L. Mills, X. Chen, P. Ray, J. He, B. Dhandapani, *Thermochim. Acta*, 406 (2003) 35.
43. R. Mills, B. Dhandapani, M. Nansteel, J. He, T. Shannon, A. Echezuria, *Int. J. Hydrogen Energy* 26 (2001) 339.
44. R. Mills, B. Dhandapani, M. Nansteel, J. He, A. Voigt, *Int. J. Hydrogen Energy* 26 (2001) 965.
45. R. Mills, B. Dhandapani, N. Greenig, J. He, *Int. J. Hydrogen Energy* 25 (2000) 1185.
46. R. L. Mills, P. Ray, *J. Phys. D Appl. Phys.* 36 (2003) 1535.
47. R. L. Mills, P. Ray, B. Dhandapani, M. Nansteel, X. Chen, J. He, *J. Mol. Struct.* 643 (2002) 43.
48. R. Mills, P. Ray, *Int. J. Hydrogen Energy* 27 (2002) 301.
49. R. L. Mills, P. Ray, *Int. J. Hydrogen Energy* 28 (2003) 825.

50. R. Mills, *Int. J. Hydrogen Energy* 26 (2001) 1041.
51. R. Mills, P. Ray, R. M. Mayo, *IEEE Trans. Plasma Sci.* 31 (2003) 236.
52. R. L. Mills, P. Ray, *J. Phys. D Appl. Phys.* 36 (2003) 1504.
53. R. Mills, P. Ray, R. M. Mayo, *Appl. Phys. Lett.* 82 (2003) 1679.
54. R. Mills, W. Good, R. Shaubach, *Fusion Technol.* 25 (1994) 103.
55. M. C. Bradford, J. Phillips, J. Klanchar, *Rev. Sci. Instrum.* 66 (1995) 171.
56. R. Mills, W. Good, *Fusion Technol.* 28 (1995) 1697.
57. R. Mills, S. Kneizys, *Fusion Technol.* 20 (1991) 65.
58. J. Niedra, I. Meyers, G.C. Fralick, R. Baldwin, "Replication of the Apparent Excess Heat Effect in a Light Water-Potassium Carbonate-Nickel Electrolytic Cell," NASA Technical Memorandum 107167, February, 1996, p. 1;  
Niedra, J., Baldwin, R., Meyers, I., NASA Presentation of Light Water Electrolytic Tests, May 15, 1994.
59. E. D. Becker, *High Resolution NMR Theory and Chemical Applications*, Second Edition, Academic Press, Inc., Orlando, 1980, pp. 20-22, 184-198.

Table 1. A summary of the  $K_2CO_3$  electrolysis parameters and power balance results with constant and intermittent current.

Experiment	Frequency (Hz)	Duty cycle (%)	$I_{pk}$ (A)	$V_{pk}$ (V)	$\eta$	$P_{cell}$ (W) Eqs. (12) and (19)	$P_T$ (W) Eq. (21)	$P_T/P_{cell}$	$Q_{xs}$ (W) Eq. (22)
$K_2CO_3$ DC	DC	100	1.72	3.02	0.66	3.51	4.06	1.16	0.55
$K_2CO_3$ pulsed	10	30	0.658	2.35	0	0.460	0.644	1.40	0.184

Fig. 1. Schematic cross sectional view of the Calvet calorimeter and  $K_2CO_3$  electrolysis cell used to measure the energy balances of the  $K$  catalyst reaction to form hydrinos. The components were: 1—Pyrex cell cap with electrolysis power feed-throughs and gas vent; 2—O-ring gasket; 3—Pyrex electrolysis cell body; 4—nickel electrolysis electrode assembly; 5—stainless steel Calvet housing and heat sink; 6—Calvet thermopile output; 7—thermal shunt and cell support manifold, and 8—Calvet thermopile responsive to power flow.

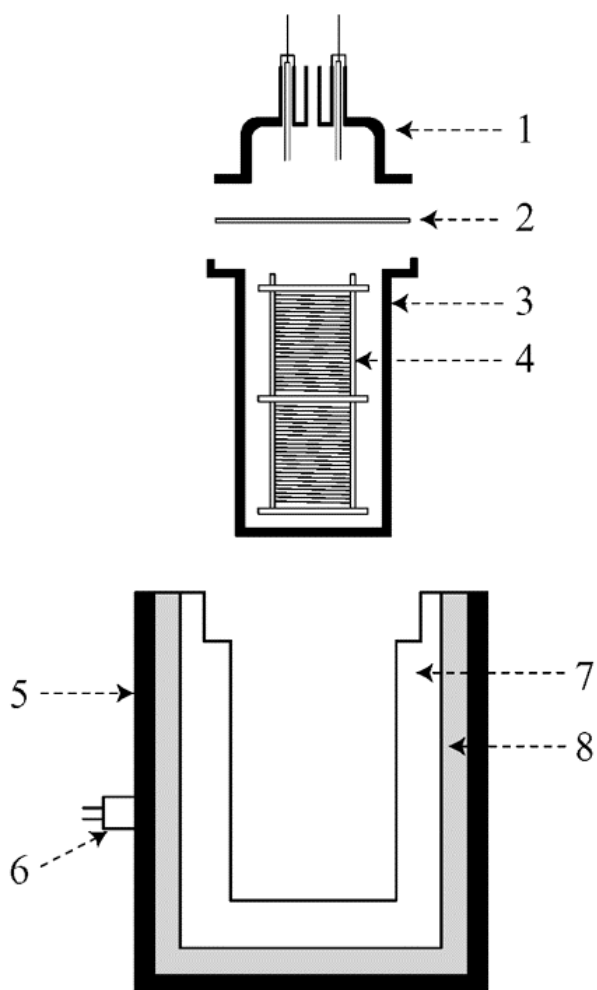


Fig. 2. Nickel wire cathode that fit inside of the nickel wire anode.



Fig. 3. Plots of the Calvet output versus ohmic input power. (Top) Pulsed-power  $K_2CO_3$  electrolysis with a nickel wire cathode and anode experiments at 10 Hz, 30% duty cycle, and 0.758 A peak current. (Bottom) Resistive heater alone working in  $K_2CO_3$ . The Calvet calibration constant  $a$  and offset  $C$  determined by applying increments of applied heating power were 0.534 V/W and 0.000 V, respectively. With a  $P_{cell}$  of 0.460 W, the production of excess power of 0.184 W was observed that was 1.40 times  $P_{cell}$ .

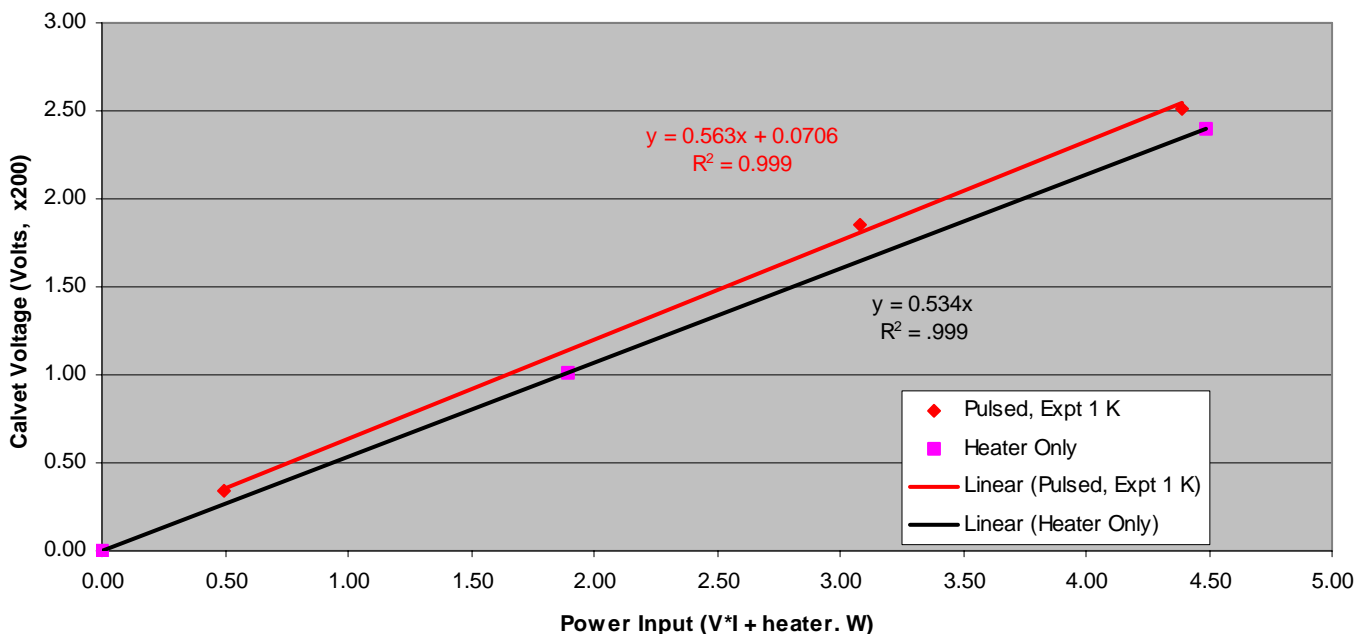


Fig. 4. The voltage and current waveforms for intermittent square-wave electrolysis recorded with a 300 MHz digital oscilloscope showing a pulse rate of 10 Hz, 30% duty cycle, and 0.758 A peak current.

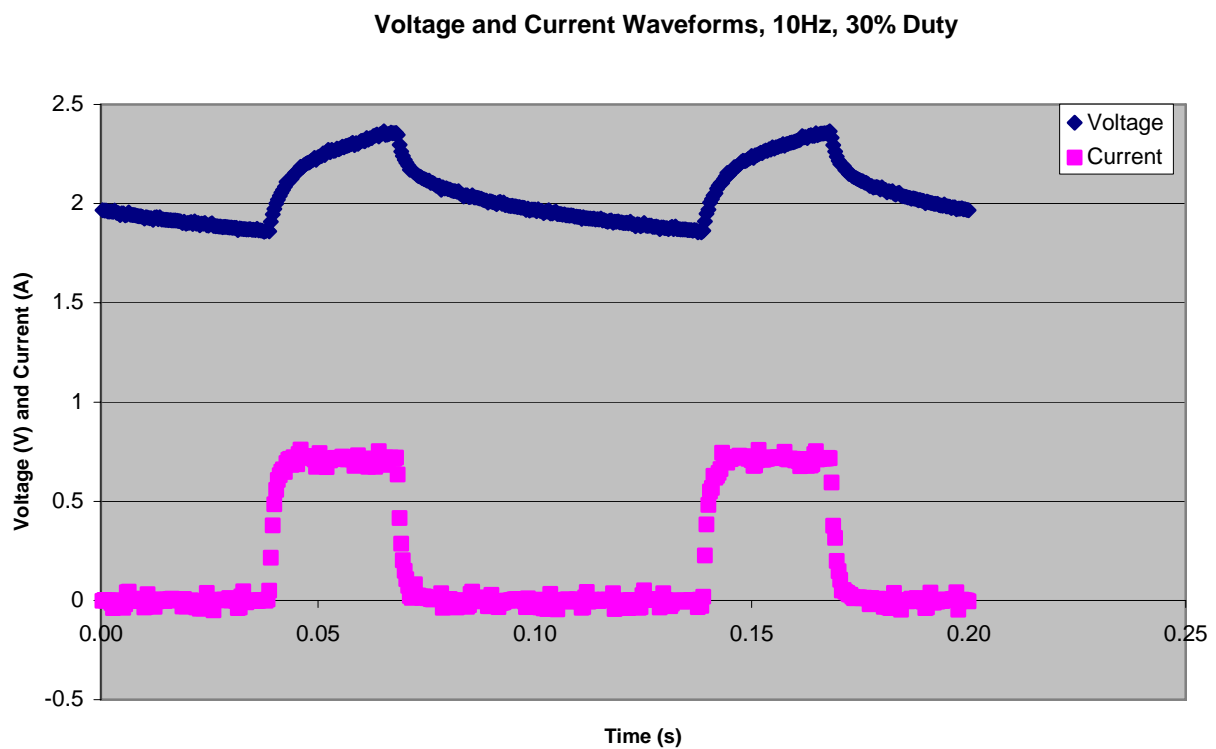


Fig. 5a-b.  $^1\text{H}$  NMR of  $\text{K}_2\text{CO}_3$  electrolysis gases collected for 5 days and dissolved in  $\text{CDCl}_3$  showing isolated  $\text{H}_2(1/4)$  at 1.25 ppm. (a) 0 ppm to 8 ppm region showing the major peaks: the solvent peak at 7.26 ppm, the  $\text{H}_2$  peak at 4.63 ppm, the acetone peak at 2.18 ppm, and the broad  $\text{H}_2\text{O}$  peak at 1.54 ppm. (b) 0.1 ppm to 1.4 ppm region showing a broad singlet peak upfield of  $\text{H}_2$  at 1.25 ppm. The 1.25 ppm peak was the only peak in the spectrum that could not be assigned to common species. It matched the theoretical position of  $\text{H}_2(1/4)$ .

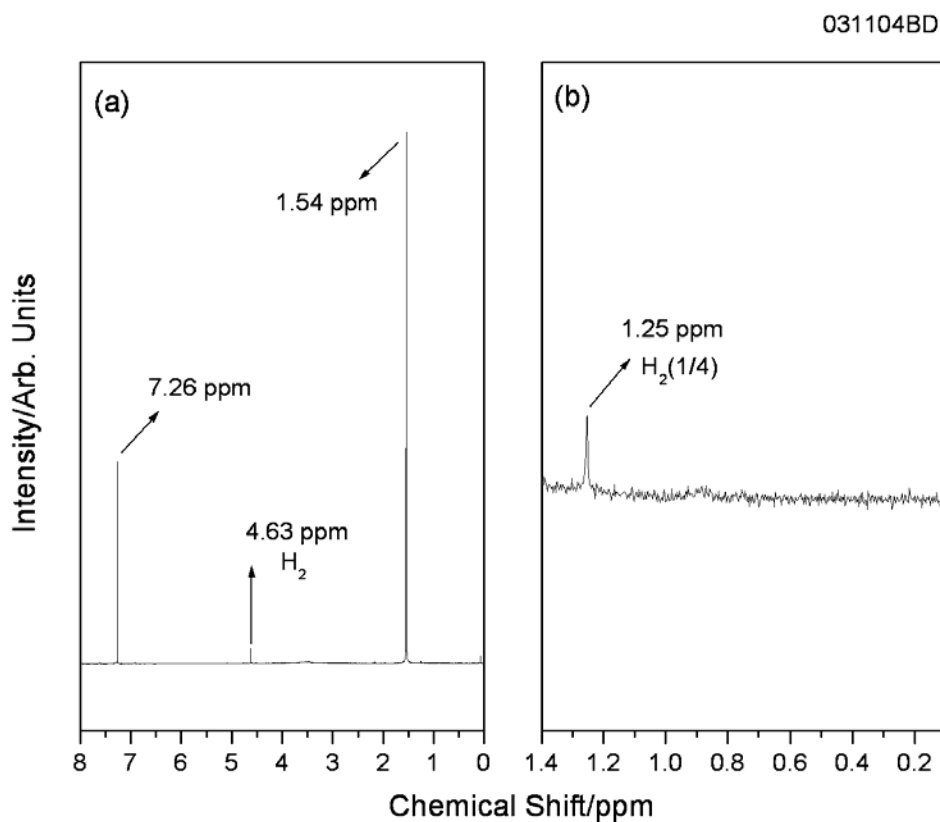


Fig. 6a-b.  $^1\text{H}$  NMR of crystals that were precipitated from the  $\text{K}_2\text{CO}_3$  electrolyte and dissolved in  $\text{CDCl}_3$  showing isolated  $\text{H}_2(1/4)$  at 1.25 ppm. (a) 0–8 ppm region showing the major peaks: the solvent peak at 7.26 ppm and the broad  $\text{H}_2\text{O}$  peak at 1.55 ppm. (b) 0–1.4 ppm region showing the broad  $\text{H}_2(1/4)$  singlet peak upfield of  $\text{H}_2$  at 1.25 ppm.

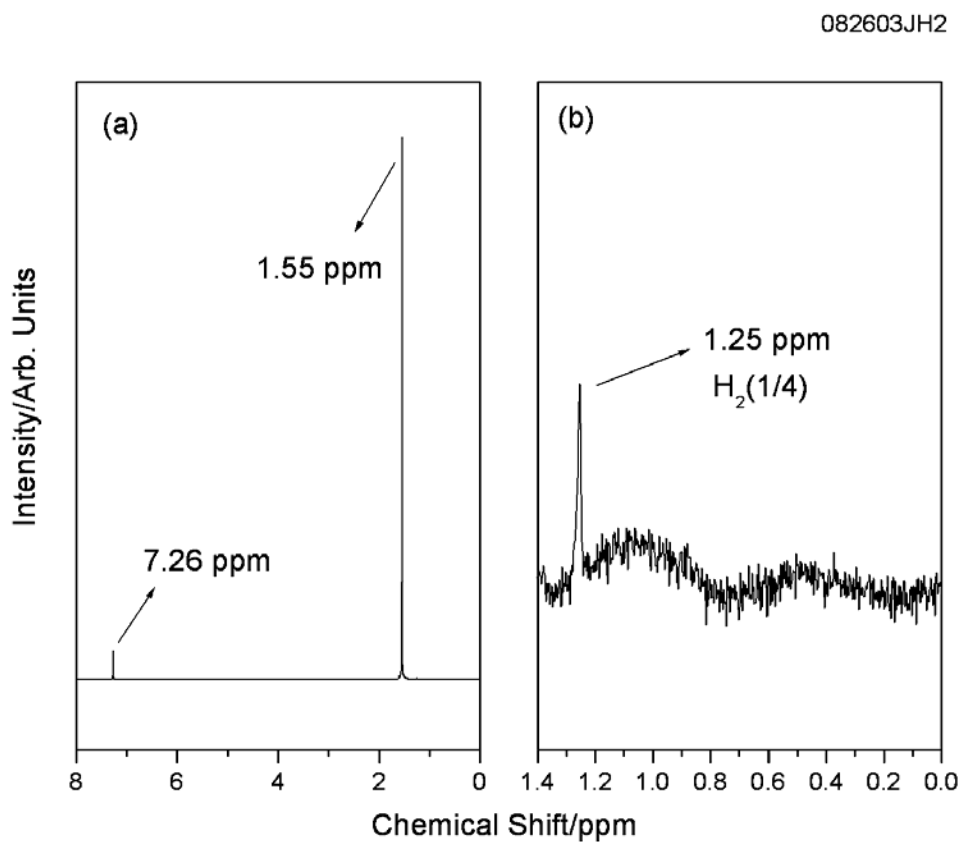


Fig. 7a-b. Figures 7a-b.  $^1\text{H}$  NMR of concentrated  $\text{K}_2\text{CO}_3$  electrolyte dissolved in  $\text{CDCl}_3$  showing isolated  $\text{H}_2(1/4)$  at 1.25 ppm. (a) 0–8 ppm region showing the major peaks: the solvent peak at 7.26 ppm and the broad  $\text{H}_2\text{O}$  peak at 1.57 ppm. (b) 0–1.4 ppm region showing the broad  $\text{H}_2(1/4)$  singlet peak upfield of  $\text{H}_2$  at 1.25 ppm.

